

Review

Thermodynamic, Dynamic, and Transport Properties of Quantum Spin Liquid in Herbertsmithite from an Experimental and Theoretical Point of View

Vasily R. Shaginyan ^{1,2,*} , Alfred Z. Msezane ², Miron Ya. Amusia ^{3,4} , John W. Clark ^{5,6},
George S. Japaridze ², Vladimir A. Stephanovich ⁷ and Yulya S. Leevik ⁸

¹ Petersburg Nuclear Physics Institute of NRC “Kurchatov Institute”, 188300 Gatchina, Russia

² Clark Atlanta University, Atlanta, GA 30314, USA

³ Racah Institute of Physics, Hebrew University, Jerusalem 91904, Israel

⁴ Ioffe Physical Technical Institute, RAS, 194021 St. Petersburg, Russia

⁵ McDonnell Center for the Space Sciences & Department of Physics, Washington University, St. Louis, MO 63130, USA

⁶ Centro de Investigação em Matemática e Aplicações, University of Madeira, 9020-105 Funchal, Madeira, Portugal

⁷ Institute of Physics, Opole University, Oleska 48, 45-052 Opole, Poland

⁸ Department of Finance, National Research University Higher School of Economics, 194100 St. Petersburg, Russia

* Correspondence: vrshag@thd.pnpi.spb.ru

Received: 15 June 2019; Accepted: 31 July 2019; Published: 7 August 2019



Abstract: In our review, we focus on the quantum spin liquid (QSL), defining the thermodynamic, transport, and relaxation properties of geometrically frustrated magnet (insulators) represented by herbertsmithite $\text{ZnCu}_3(\text{OH})_6\text{Cl}_2$. The review mostly deals with an historical perspective of our theoretical contributions on this subject, based on the theory of fermion condensation closely related to the emergence (due to geometrical frustration) of dispersionless parts in the fermionic quasiparticle spectrum, so-called flat bands. QSL is a quantum state of matter having neither magnetic order nor gapped excitations even at zero temperature. QSL along with heavy fermion metals can form a new state of matter induced by the topological fermion condensation quantum phase transition. The observation of QSL in actual materials such as herbertsmithite is of fundamental significance both theoretically and technologically, as it could open a path to the creation of topologically protected states for quantum information processing and quantum computation. It is therefore of great importance to establish the presence of a gapless QSL state in one of the most prospective materials, herbertsmithite. In this respect, the interpretation of current theoretical and experimental studies of herbertsmithite are controversial in their implications. Based on published experimental data augmented by our theoretical analysis, we present evidence for the existence of a QSL in the geometrically frustrated insulator herbertsmithite $\text{ZnCu}_3(\text{OH})_6\text{Cl}_2$, providing a strategy for unambiguous identification of such a state in other materials. To clarify the nature of QSL in herbertsmithite, we recommend measurements of heat transport, low-energy inelastic neutron scattering, and optical conductivity $\bar{\sigma}$ in $\text{ZnCu}_3(\text{OH})_6\text{Cl}_2$ crystals subject to an external magnetic field at low temperatures. Our analysis of the behavior of $\bar{\sigma}$ in herbertsmithite justifies this set of measurements, which can provide a conclusive experimental demonstration of the nature of its spinon-composed quantum spin liquid. Theoretical study of the optical conductivity of herbertsmithite allows us to expose the physical mechanisms responsible for its temperature and magnetic field dependence. We also suggest that artificially or spontaneously introducing inhomogeneity at nanoscale into $\text{ZnCu}_3(\text{OH})_6\text{Cl}_2$ can both stabilize its QSL and simplify its chemical preparation, and can provide for tests that elucidate the role of impurities. We make predictions of the results of specified measurements related to the dynamical, thermodynamic, and transport properties in the case of a gapless QSL.

Keywords: quantum spin liquids; herbertsmithite; fermion condensation; topological quantum phase transitions; flat bands

PACS: 64.70.Tg; 75.40.Gb; 78.20.-e; 71.10.Hf

1. Introduction

The frustrated magnet (insulator) herbertsmithite $\text{ZnCu}_3(\text{OH})_6\text{Cl}_2$ is one of the best candidates for identification as a material that hosts a quantum spin liquid (QSL), thereby determining the nature of its thermodynamic, relaxation, and transport properties. The insulating nature of $\text{ZnCu}_3(\text{OH})_6\text{Cl}_2$ has been established: There is a 3.3 eV charge gap (see e.g., [1,2]). In our review, we focus on a spin gap of QSL, and for brevity will call it “spin gap”. At low temperatures T , a QSL may have or may not have a gap in its excitation spectrum of spinons, which are fermion quasiparticles of zero charge that occupy the corresponding Fermi sphere with Fermi momentum p_F . We note that, in contrast to metals, spinons cannot support charge current, but these, for instance, can carry heat, as electrons of metals do. The influence of a gap on the properties is huge, for at low T the properties of herbertsmithite are similar to those of common insulators, while the properties resemble those of metals, provided that the gap is absent. Thus, it is a challenge to experimentally establish the presence of the gap and its value, for current theoretical and experimental studies of herbertsmithite are controversial and cannot give a definite answer to the challenge. In the present review, based primarily on our own theoretical work, we offer a number of experiments that can discern unambiguously the presence of a gapless QSL in $\text{ZnCu}_3(\text{OH})_6\text{Cl}_2$ and other geometrically frustrated magnets. Our aim here is to let the readers to make their own qualified judgments about the presented theoretical approach and its ability to deliver an adequate description of many seemingly different experiments in a uniform manner.

In a magnet with geometric frustration, where the spins cannot be ordered even at temperatures close to absolute zero, they stay in a liquid quantum spin state. Herbertsmithite is an antiferromagnet with a kagome lattice of spins $S = 1/2$. Recent experimental studies have shown its unusual properties [3–8].

The balance of electrostatic forces for the Cu^{2+} ions in the kagome structure is such that they occupy distorted octahedral sites. The magnetic planes formed by the Cu^{2+} $S = 1/2$ ions are interspersed with nonmagnetic Zn^{2+} layers. In samples, Cu^{2+} defects occupy the nonmagnetic Zn^{2+} sites between the kagome layers with $x \simeq 15\%$ probability, thus introducing randomness and inhomogeneity into the lattice [9]. As we shall see, the starring role of impurities in the formation of QSL is not clearly understood and is now under thorough investigation [10–15]. However, we suggest that the influence of impurities induced by the homogeneity on the properties of $\text{ZnCu}_3(\text{OH})_6\text{Cl}_2$ can be tested by varying x . We note that the impurities randomly located at the nanoscale level can support QSL as it is observed in measurements on $\text{Zn}_x\text{Cu}_{4-x}\text{OH}_6\text{Cl}_2$ with $1 \geq x \geq 0.8$, while at $x > 0.8$, glassy dynamics emerge [5]. Moreover, the impurities randomly located at the nanoscale level can stabilize QSL as it is observed in measurements on the verdazyl-based complex $\text{Zn}(\text{hfac})_2(\text{A}_x\text{B}_{1-x})$ [15] and make QSL stable in highly magnetic fields, as in the case of Mg-doped $\text{SrCu}_2(\text{BO}_3)_2$ [14].

The experiments done on $\text{ZnCu}_3(\text{OH})_6\text{Cl}_2$ have not found any traces of magnetic order in it. Nor they have found the spin freezing down to temperatures of around 50 mK. In these respects, herbertsmithite is the best candidate among quantum magnets to contain QSL described above [3–8]. These assessments are supported by model calculations indicating that an antiferromagnet on a kagome lattice has a gapless spin liquid ground state [16–23]. At the same time, recent suggestions [9,24,25] that there can exist a small spin-gap in the kagome layers may stand in conflict to this emerging picture (see also refs. [26–28] for a recent review). The obtained results are a combination of experimental and theoretical ones. The latter have been obtained in the framework of the model, which takes the presence of Cu impurities into account. The experimental data has been obtained by inelastic neutron

scattering on $\text{ZnCu}_3(\text{OH})_6\text{Cl}_2$ crystals. It is assumed that the influence of the Cu impurity ensemble on the observed properties of herbertsmithite may be disentangled from that of the kagome lattice geometry [9,24,25]. It is further assumed that the impurity ensemble may be represented as a result of the dilution of some prototypic cubic lattice. The model supposes that the spin gap occurs in magnetic fields up to 9 T. We note that measurements of the local spin susceptibility of $\text{ZnCu}_3(\text{OH})_6\text{Cl}_2$ show that the kagome spins exhibit a spin gap [24], while the measurements of the bulk spin susceptibility evidence the absence of the gap [3]. We shall see below that it is not possible to separate contributions coming from the local and bulk susceptibility, for both the kagome and the impurities spins form an integral system.

At the same time, without a magnetic field, the spin susceptibility χ shows behavior in many respects similar to the Curie law. The latter behavior demonstrates that the copper spin ensemble plays the role of weakly interacting impurities [9,24,25]. The same behavior was recently reported in a new kagome quantum spin liquid candidate, $\text{Cu}_3\text{Zn}(\text{OH})_6\text{FBr}$ [29]. As a result, we observe a challenging contradiction between two sets of experimental data when some of them state the absent of a gap while the others present evidence in favor of a gap. Subsequently, we shall demonstrate that the model based on the Cu spin ensemble is rather synthetic. In other words, this model does not have the possibility of distinguishing the Cu ensemble and kagome lattice contributions. This is because the impurities, being embedded in the kagome host lattice, form a single integral entity at nanoscale. The above model may contradict the accumulated knowledge about the physical properties of $\text{ZnCu}_3(\text{OH})_6\text{Cl}_2$. This knowledge is the result of vast theoretical and experimental efforts related to static and dynamic properties of herbertsmithite [3–8,16–23]. Thus, when analyzing the physics of quantum spin liquid in the herbertsmithite, it is of crucial importance to verify the existence of a spin gap by experimental and theoretical studies, for the gap strongly influences all its thermodynamic, transport, and relaxation properties. To analyze QSL behavior theoretically, we employ the strongly correlated quantum spin liquid (SCQSL) [16–18,20,23] model. A simple kagome lattice may host a dispersionless topologically protected branch of the quasiparticle spectrum with zero excitation energy, known as a flat band [16,18,23,30–32]. In that case, the topological fermion condensation quantum phase transition (FCQPT) can be considered as a quantum critical point (QCP) of the $\text{ZnCu}_3(\text{OH})_6\text{Cl}_2$ spinon-composed QSL. Spinons have zero charge, occupying the Fermi sphere up to the Fermi momentum p_F [16,17,32]. Taking into account that we are dealing with the real chemical compound $\text{ZnCu}_3(\text{OH})_6\text{Cl}_2$ rather than with an ideal kagome lattice, we have to bear in mind that the actual magnetic interaction in the compound can shift QSL away from FCQPT, before or beyond QCP. Thus, the actual critical point location has to be established by experimental data analysis. The real part of the optical conductivity $\bar{\sigma}$, measured at low frequency on geometrically frustrated magnetic insulators, can yield important experimental clues to the nature of spinon-based QSL [33,34], especially at a wide range of temperatures T and magnetic fields B . Note that the consistent interpretation of the above data is a difficult theoretical problem [33].

The main aim of the present review is to expose QSL as a new state of matter, also formed by heavy fermion (HF) metals, and to attract attention to experimental studies of $\text{ZnCu}_3(\text{OH})_6\text{Cl}_2$ that have the potential to reveal both the underlying physics of QSL and the presence or absence of a gap in spinon excitations that form the thermodynamic, transport, and relaxation properties. To clarify the nature of QSL in herbertsmithite, we recommend measurements of heat transport, low-energy inelastic neutron scattering, and optical conductivity $\bar{\sigma}$ in $\text{ZnCu}_3(\text{OH})_6\text{Cl}_2$ single crystals subject to an external magnetic field at low temperatures. We show that QSL is situated near FCQPT, which stems from the dependence of $\bar{\sigma}$ on the external magnetic field. We argue that the general physical picture inherent in QSL can be “purified” of the microscopic contributions coming both from phonons and the impurities polluting each specific sample being studied. We suggest that the influence of impurities on the properties of $\text{ZnCu}_3(\text{OH})_6\text{Cl}_2$, induced by the inhomogeneity, can be tested by varying x .

In the following sections on thermodynamic properties, relaxation, and optical conductivity, we shall demonstrate that the existence of a gap within the impurity model of herbertsmithite may

contradict recent experimental data collected on this material; instead, the impurities and kagome planes can form a genuine SCQSL. Accordingly, the observed gap [24] related to the kagome planes may not be a real one as it is not a physical mechanism for the observed thermodynamic, relaxation, and conductivity properties of $\text{ZnCu}_3(\text{OH})_6\text{Cl}_2$.

2. Frustrated Insulator Herbertsmithite

If the quasiparticles forming QSL are approximately dispersionless spinons (uncharged fermions), this state of matter becomes an SCQSL, [17,18,20,35,36]. If an insulating chemical compound has a 2D lattice, an SCQSL can emerge as a result of the lattice geometrical frustration. Most frequently, such frustration results in a dispersionless topologically protected spectral branch with zero excitation energy, called a flat band. This scenario realizes in herbertsmithite with its kagome planes [18,30,32,37–39], shown in Figure 1a. In this case, SCQSL has its quantum critical point at the FCQPT. As we have mentioned above, the SCQSL consists of chargeless $S = 1/2$ spinons having the effective mass M^* . Their momenta, as usual for fermions, reside in a Fermi sphere with momentum p_F . Note that one frustrated valence spin is taken away to populate the approximately flat spinon band, as is displayed in Figure 1b. Such a behavior strongly resembles that of HF metals whose valence electrons form conduction flat bands, while the charges $-e$ cannot form any band because of the large charge gap of herbertsmithite or another geometrically frustrated insulating magnet. This result is in agreement with the experimental data [40]. Therefore, the above insulating compounds have physical properties resembling those of HF metals. There is, however, a notable exception. Namely, while HF metals are good conductors, the typical insulator does not sustain the electric current [18–20]. Thus, both frustrated insulators and HF metals, having universal behavior, form a new state of matter [35].

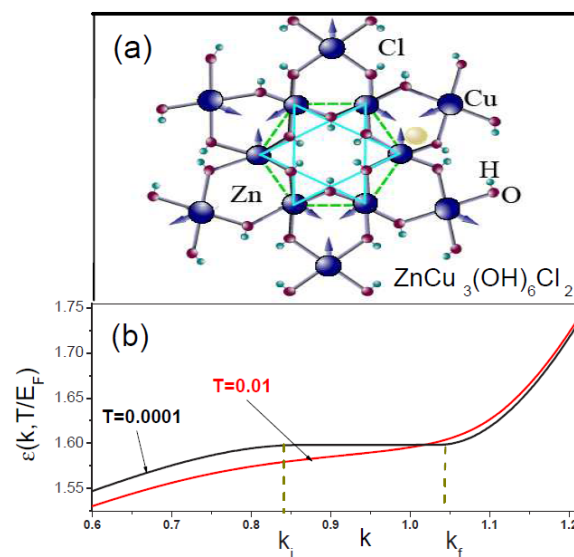


Figure 1. Kagome lattice and flat band. Panel (a) Crystal structure of $\text{ZnCu}_3(\text{OH})_6\text{Cl}_2$ along the hexagonal c axis. The blue spheres are Cu sites. Arrows show Cu spins in the frustrated configuration. The kagome planes with frustrated spins, occupying a flat band (panel (b)), are shown by two triangles and highlighted by the dashed lines, displaying the hexagon. Groups of OH, Zn, and Cl atoms are shown schematically. Zn atoms may be situated below or above Cu planes. Panel (b) Calculated single particle spectrum $\epsilon(k, T/E_F)$ as a function of dimensionless momentum $k = p/p_F$ and temperature T/E_F , with E_F being the Fermi level [16,17]. The cases of almost zero ($T = 10^{-4}E_F$; black curve) and finite ($T = 10^{-2}E_F$; red curve) temperatures are reported. It is seen that the dispersionless part of the spectrum vanishes at finite temperatures, making the situation almost indistinguishable from normal Fermi liquid, while at $T \rightarrow 0$ the band becomes almost flat at $k_i < k < k_f$, where $k_i = p_i/p_F$ and $k_f = p_f/p_F$.

3. Thermodynamic Properties

If QSL-forming quasiparticles are approximately dispersionless spinons (uncharged fermions), this state of matter becomes an SCQSL [17,18,20,35,36]. As we have mentioned above, the geometrical frustration in herbertsmithite promotes the SCQSL formation [18–20], while the presence of randomly scattered impurities can facilitate the frustration (see e.g., [15]). Note that in real chemical compounds with many lattice imperfections, the actual SCQSL emergence point is shifted from the theoretically predicted FCQPT. This means that the mutual location of the SCQSL and FCQPT can only be extracted from the experimental data.

Famous Fermi liquid theory, proposed by Landau (the so-called Landau Fermi liquid (LFL) theory) [41], has de facto been the universal tool to describe the itinerant fermionic systems. It maps the ensemble of strongly interacting electrons in a solid to the effective quasiparticle gas with not so strong an interaction. In such an approach, the excitations are represented in terms of the above quasiparticles so that the low-temperature properties of the system under consideration depend on the latter. The quasiparticles possess certain effective mass M^* , which is a parameter of the theory [41–43], being approximately independent of external stimuli including temperature, pressure, or an electromagnetic field. The LFL theory cannot, however, explain the experimental results related to strong temperature and/or magnetic field dependence of the effective mass M^* , as observed in strongly correlated Fermi systems [16,44]. At the same time, deviations from LFL behavior are observed in the vicinity of an FCQPT [16,17,44]. The above peculiarities are usually addressed as non-Fermi-liquid (NFL) properties. They are due to large effective mass, which actually becomes infinite at the FCQPT point (see [16,17] for details).

Let us describe the physical mechanism yielding the temperature and field dependences of the effective mass of the Landau quasiparticle $M^*(B, T)$. Again, the key point is that upon approach to the FCQPT from the LFL regime, the effective mass becomes strongly external-stimuli-dependent. The aforementioned stimuli are the temperature, the magnetic field, and the external pressure P , to name a few [16,17]. This is indeed a consequence of an additional instability channel of a normal Fermi liquid (to those of Pomeranchuk, [42]). Note that the new channel is activated when the effective mass approaches infinity.

To avoid unphysical situations related, for instance, to the negativity of the effective mass, the system alters the topology of its Fermi surface [32,38,39] so that the effective mass starts to depend on the above external stimuli [16,17]. For our studies of the effective mass properties in SCQSL, we adopt the so-called homogeneous Fermi liquid model. Such a description avoids consideration of nonuniversal (and highly irrelevant in our analysis) features like the exact structure of a specific sample [16,17]. In such a model, the LFL equation for $M^*(B, T)$ reads [16,17,41]

$$\frac{1}{M^*(B, T)} = \frac{1}{M} + \sum_{\sigma_1} \int \frac{\mathbf{p}_F \cdot \mathbf{p}}{p_F^3} F(\mathbf{p}_F, \mathbf{p}) \times \frac{\partial n_{\sigma_1}(\mathbf{p}, T, B)}{\partial p} \frac{d\mathbf{p}}{(2\pi)^3}. \quad (1)$$

In this expression, M is the free electron mass, $F(\mathbf{p}_F, \mathbf{p})$ is the Landau interaction function, depending on p (momentum), p_F (constant Fermi momentum), and $n_{\sigma}(\mathbf{p}, T, B)$, which is the quasiparticle distribution function for the spin projection σ . The quasiparticle interaction $F(\mathbf{p}, \mathbf{p}_1)$, assumed here to be spin-independent, is phenomenological. Without loss of generality, here we assume that $F(\mathbf{p}, \mathbf{p}_1)$ is independent of temperature so that $n_{\sigma}(\mathbf{p}, T)$ has the Fermi–Dirac form

$$n_{\sigma}(\mathbf{p}, T) = \left\{ 1 + \exp \left[\frac{(\varepsilon_{\sigma}(\mathbf{p}, T) - \mu_{\sigma})}{T} \right] \right\}^{-1}, \quad (2)$$

where $\varepsilon_\sigma(\mathbf{p}, T)$ is a single-particle energy spectrum. In addition, μ is a chemical potential, which is spin-dependent via Zeeman splitting $\mu_\sigma = \mu \pm \mu_B B$, where μ_B is the Bohr magneton. As usual, the spectrum $\varepsilon_\sigma(\mathbf{p}, T)$ is obtained variationally from the system energy $E[n_\sigma(\mathbf{p}, T)]$,

$$\varepsilon_\sigma(\mathbf{p}, T) = \frac{\delta E[n(\mathbf{p})]}{\delta n_\sigma} \tag{3}$$

In describing herbertsmithite as a strongly correlated quantum spin liquid, the choice of the function $F(\mathbf{p}, \mathbf{p}_1)$ is dictated by its possession of FCQPT [16]. Thus, the sole role of the Landau interaction is to drive the system to the FCQPT point, at which the topology of the Fermi surface is altered in such a way that the effective mass ceases to be a constant parameter obtaining the aforementioned dependence on external stimuli [16,17]. Performing the variation (3), we arrive at the expression for a single-particle energy spectrum

$$\frac{\partial \varepsilon_\sigma(\mathbf{p}, T)}{\partial \mathbf{p}} = \frac{\mathbf{p}}{M} - \int \frac{\partial F(\mathbf{p}, \mathbf{p}_1)}{\partial \mathbf{p}} n_\sigma(\mathbf{p}_1, T) \frac{d^3 p_1}{(2\pi)^3} \tag{4}$$

Equations (2) and (4) constitute the closed set to find $\varepsilon_\sigma(\mathbf{p}, T)$ and $n_\sigma(\mathbf{p}, T)$. In this case, the effective mass enters through the expression $p_F/M^* = \partial \varepsilon(p)/\partial p|_{p=p_F}$. At the FCQPT point, the analytical solution of Equation (1) is possible [16,17]. Namely, in contrast to the LFL approach with M^* being a constant parameter, here at zero magnetic field, M^* becomes temperature dependent. The latter feature comprises the strong deviation from the LFL picture, determining the NFL regime

$$M^*(T) \simeq a_T T^{-2/3} \tag{5}$$

At elevated temperatures, the system undergoes a transition to the LFL region of the phase diagram, and being subjected to the magnetic field, exhibits the behavior

$$M^*(B) \simeq a_B B^{-2/3} \tag{6}$$

of the effective mass.

The introduction of “internal” (or natural) scales greatly simplifies the analysis of the problem under consideration. We first observe that near the FCQPT, the effective mass $M^*(B, T)$ (i.e., the solution to Equation (1)) has a maximum M_M^* at a temperature $T_M \propto B$ [16,17]. This means that it is convenient to measure the effective mass and temperature in the units M_M^* and T_M , respectively. Thus, we arrive at normalized effective mass $M_N^* = M^*/M_M^*$ and temperature $T_N = T/T_M$. Near FCQPT, the dependence $M_N^*(T_N)$ can be rendered as a universal interpolating function [16,17]. This function describes the transition from LFL to NFL states, given by Equations (5) and (6), and presents the universal scaling behavior of M_N^* [16,17]

$$M_N^*(y) \approx c_0 \frac{1 + c_1 y^2}{1 + c_2 y^{8/3}} \tag{7}$$

Here, $y = T_N = T/T_M$ and $c_0 = (1 + c_2)/(1 + c_1)$, where c_1 and c_2 are free parameters. The magnetic field B enters Equation (1) only in the combination $\mu_B B/T$, making $T_M \sim \mu_B B$. It follows from Equation (7) that

$$T_M \simeq a_1 \mu_B B, \tag{8}$$

where a_1 is a dimensionless quantity. In this case, the variable y becomes $y = T/T_M \sim T/\mu_B B$. The Equation (8) permits us to assert Equation (7), giving the scaling properties of temperature and magnetic field dependence of the effective mass. This implies, in turn, that at different fields B ,

the curves M_N^* form a single one as a function of the normalized variable $y = T/T_M$. As T and B enter symmetrically in Equation (7), it also manifests the scaling behavior of $M_N^*(B, T)$ as a function of T/B :

$$T_N = \frac{T}{T_M} = \frac{T}{a_1 \mu_B B} \propto \frac{T}{B} \propto \frac{B}{T}. \quad (9)$$

The schematic phase diagram is portrayed in Figure 2. We assume for simplicity that at $T = 0$ and $B = 0$, the system is near FCQPT. The external magnetic field and temperature are indeed the parameters controlling the system position on the phase diagram relatively to the FCQPT point. The same parameters are responsible for the transitions between the NFL and LFL regions of the phase diagram (see the arrows in Figure 2). The horizontal arrow corresponds to fixed temperatures so that the system motion along this arrow from the NFL to LFL region corresponds to a magnetic field increase. On the contrary, the vertical arrow fixes the magnetic field so that the motion along it signifies the elevated temperatures. The shaded area reports the region where the NFL state transits to a weakly polarized LFL one. The temperature $T^*(B)$ of the transition is defined by the expression

$$T^*(B) \simeq T_M(B), \quad (10)$$

which directly follows from Equation (8). The line Equation (10) is indeed the function $T^* \propto \mu_B B$, so that the width $W(B)$ of the NFL region is proportional to the temperature. It can be shown similarly that the transition region width $T^W(B)$ is also $\propto T$ [16,17]. We note here that in essence, the transition region represents the crossover between LFL and NFL phases. In our case, the NFL phase is formed by quasiparticles that occupy the so-called fermion condensate (FC) state, in analogy to the Bose condensate for particles obeying Bose–Einstein statistics. (See [16,17] for a comprehensive explanation.) In a “pure” FC state, all fermions (quasiparticles) having momenta in a finite interval embracing the Fermi surface have energies pinned to the chemical potential. In reality, this state cannot be reached because of the Nernst theorem [45], and the NFL features arise from “traces” of the FC state manifested at finite temperatures. Moreover, at low but finite temperatures, the magnetic field acts to suppress NFL behavior (i.e., the “FC traces”) and, upon growing sufficiently strong, restores the LFL phase. On the other hand, thermal fluctuations destroy LFL behavior and generate NFL features related to the FC state.

To examine the impurity model and possible gap in the spinon single particle spectrum, we consider the measured properties of herbertsmithite magnetic susceptibility χ . It is seen from Figure 3 that the magnetic susceptibility diverges as $\chi(T) \propto T^{-2/3}$ at $B \leq 1$ T (full line). For weakly interacting impurities, it has been suggested that at low temperatures, the dependence $\chi(T)$ can be approximated by a Curie–Weiss law [9,24,25], i.e., $\chi_{CW}(T) \propto 1/(T + \theta)$, where θ is a Curie temperature, which turns out to be very small. At the same time, with respect to firmly established behavior $\chi(T) \propto T^{-2/3}$ at low B , the above Curie–Weiss approximation is in discord with both theory [17,18,20] and experiment [3]. Moreover, as seen in Figure 4, the normalized spin susceptibility χ_N behaves like the normalized specific heat C_{el}/T extracted from measurements on YbRh₂Si₂ in high magnetic fields [46] and displayed in Figure 5a. Note that C_{el}/T displayed in Figure 5a coincides approximately with $C_{mag}(B, T)/T \simeq C_{el}(B, T)/T$ shown in Figure 6, pointing to similarity of the electron and spinon Fermi spheres. Figure 5b reports the normalized specific heat $(C_{el}/T)_N$ extracted from the data [46,47]. It is seen that at low magnetic fields, the electronic system is not polarized as it is at high ones (black line) [17,48]. We note that the same behavior is exhibited by both χ_N shown in Figure 6 and $(C_{mag}/T)_N$ shown in Figure 7. These facts support our conclusion that the SCQSL of ZnCu₃(OH)₆Cl₂ behaves like both the HF electron liquid of YbRh₂Si₂ and the insulator Cu(C₄H₄N₂)(NO₃)₂ [49,50].

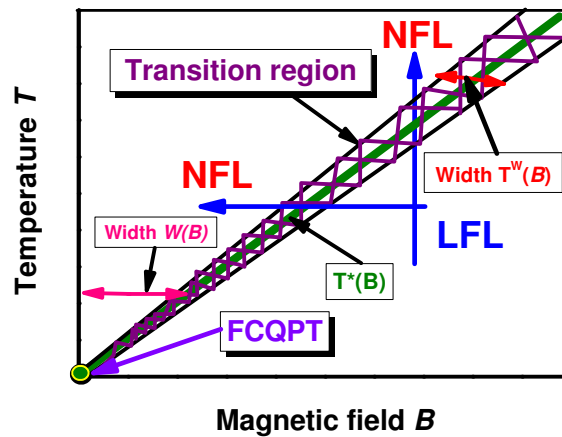


Figure 2. (Color online). Schematic strongly correlated quantum spin liquid (SCQSL) phase diagram in the “temperature–magnetic field” representation. The magnetic field B is the independent variable (control parameter). Vertical and horizontal arrows show Landau Fermi liquid (LFL)–non-Fermi-liquid (NFL) and NFL–LFL transitions at fixed B and T , respectively. The dependences $M^*(T)$ and $M^*(B)$ are given by Equations (5) and (6), respectively. The hatched area represents the transition region at $T = T^*(B)$ (see Equation (10)). The transitions occur according to the directions of the blue arrows. The solid line in the hatched area represents the function $T^*(B) \simeq T_M(B)$ given by Equation (8). The functions $W(B) \propto T \propto T^*$ and $T^W(B) \propto T \propto T^*$ shown by two-headed arrows define the width of the NFL state and the transition area, respectively. At the fermion condensation quantum phase transition (FCQPT) indicated by the arrow, the effective mass M^* diverges, and both $W(B)$ and $T^W(B)$ tend to zero.

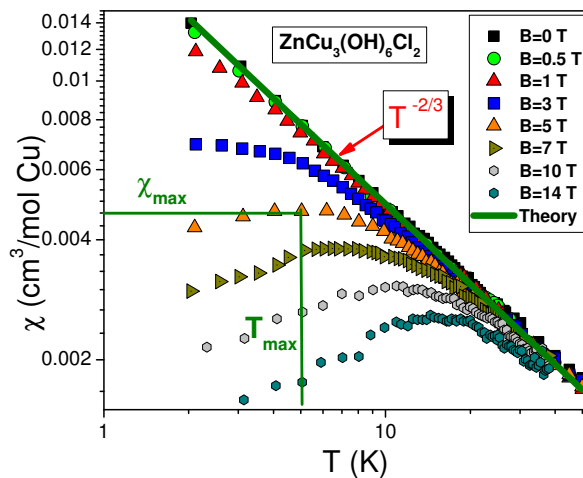


Figure 3. (Color online) The dependence $\chi(T)$, measured experimentally on $\text{ZnCu}_3(\text{OH})_6\text{Cl}_2$, taken from [3]. Magnetic fields are coded by symbols and reported in the legend. The example of χ_{max} and T_{max} at $B = 3$ T is shown. The result of calculation at $B = 0$ (full line) shows the dependence $\chi(T) \propto T^{-2/3}$ [17,18,21].

In fact, at $T = 0$, the FC state is represented by the superconducting state with the superconducting gap $\Delta = 0$, while the superconducting order parameter $\kappa = \sqrt{n(p)(1 - n(p))}$ is finite in the region $(p_i - p_f)$ [16,31,51], for in the region $n(p) < 1$.

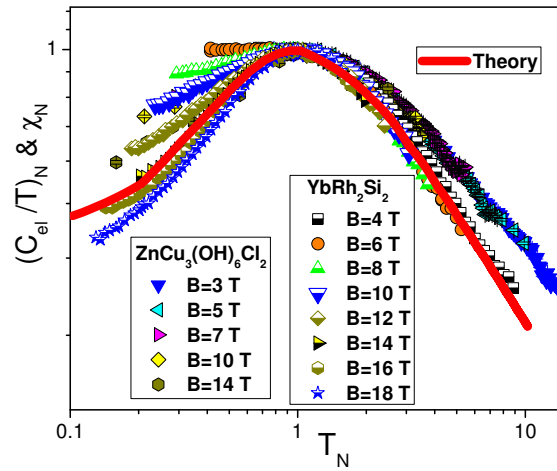


Figure 4. Normalized susceptibility $\chi_N = \chi/\chi_{max} = M_N^*$ versus normalized temperature T_N (see Equation (7)) of $ZnCu_3(OH)_6Cl_2$ [3] as collected in Figure 3. We normalize specific heat $(C_{el}/T)_N = M_N^*$ taken from the experimental results on C_{el}/T in $YbRh_2Si_2$ in magnetic fields B shown in Figure 5 (b) [46]. The corresponding values of B (legends) are coded by symbols. The full curve marks our theoretical calculations at $B \simeq B^*$ when the quasiparticle band is fully polarized. [17,20].

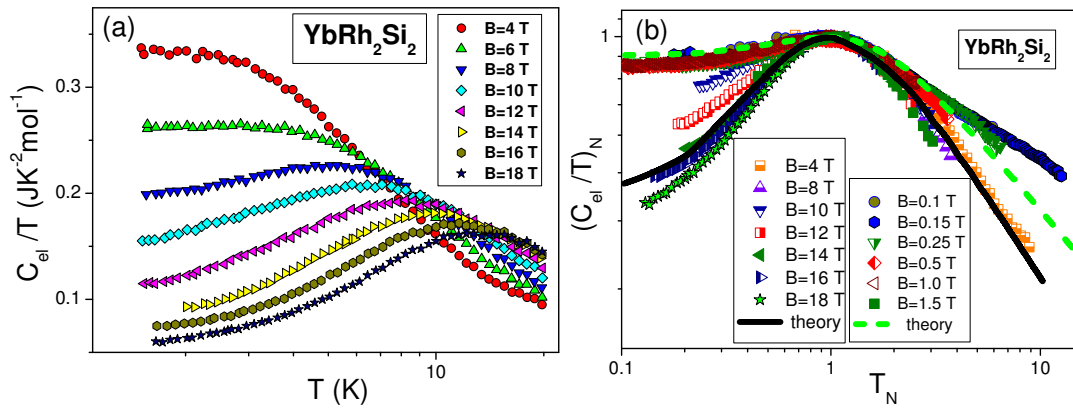


Figure 5. (Color online) Electronic specific heat C_{el}/T of the archetypical heavy fermion (HF) metal $YbRh_2Si_2$. Panel (a) reports the temperature dependence of the electronic specific heat C_{el}/T of $YbRh_2Si_2$ at high magnetic fields [46] shown in the legend. The electronic specific heat C_{el}/T of $YbRh_2Si_2$ strongly resembles C_{mag}/T of $ZnCu_3(OH)_6Cl_2$, shown in Figure 6. Panel (b): The normalized specific heat C_{el}/T at high [46] and low magnetic fields [47] extracted from the specific heat (C/T) measurements on the $YbRh_2Si_2$. The low-field calculations are depicted by the short-dash curve tracing the scaling behavior of M_N^* (see Equation (7)). Our high-field calculations (solid line) are taken at high magnetic field B , at which the quasiparticle band becomes fully polarized [48].

The above observations point to a possible absence of the spin gap in $ZnCu_3(OH)_6Cl_2$, for it is impossible to definitely separate the contributions of the impurities and of kagome planes. The impurity model implies that the intrinsic spin susceptibility of the kagome plane is decomposed as $\chi_{kag}(T) = \chi(T) - \chi_{CW}(T)$, leading to $\chi_{kag}(T \rightarrow 0) \rightarrow 0$ and the result about the existence of a putative gap [25]. This shows that there is a problem with the impurity model as it cannot describe the firmly established behavior $\chi(T) \propto T^{-2/3}$ [3]. Thus, to explain the observed behavior of χ , one should view the impurity ensemble embedded in the kagome host crystal lattice as an integral system [16–21,23,49,50,52] that acts coherently at nanoscale to produce additional frustration of the kagome planes, so as to make QSL robust at lower temperatures. Based on this analysis, we predict that QSL of quantum magnets can be stabilized by introducing a random distribution of

impurities. We also note that artificially or spontaneously introducing impurities into $\text{ZnCu}_3(\text{OH})_6\text{Cl}_2$ can both stabilize its QSL and simplify its chemical preparation.

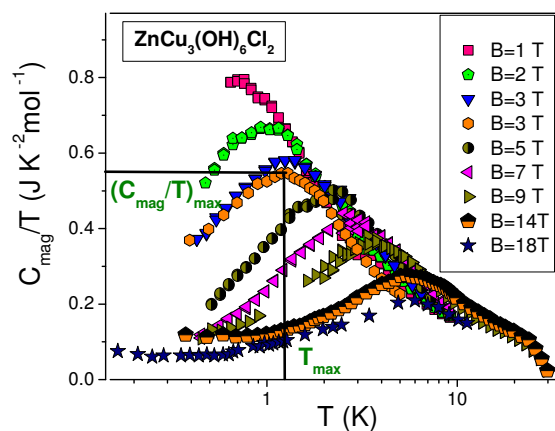


Figure 6. (Color online) Specific heat C_{mag}/T measured on powder [4,5] and single-crystal [6–8] herbertsmithite samples as a function of temperature. Magnetic fields (legend) are coded by symbols. It is clearly seen that powder and single-crystal samples have approximately the same C_{mag}/T . The example of $C_{\text{mag}}/T_{\text{max}}$ and T_{max} at $B \simeq 3$ T is shown.

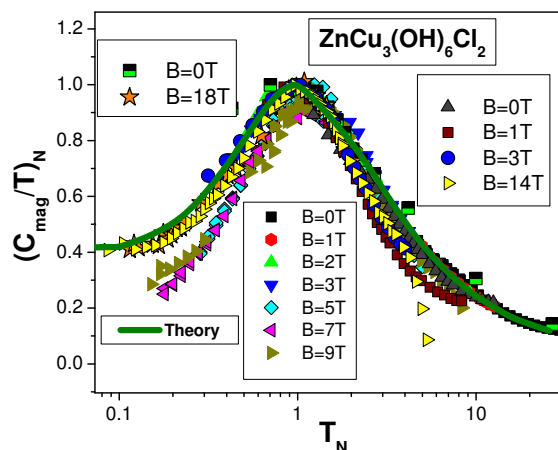


Figure 7. (Color online) Normalized specific heat $(C_{\text{mag}}/T)_N$ versus normalized temperature T_N at different magnetic fields (legend) [17,23] extracted from specific heat C_{mag}/T measured on powder [4,5] and single-crystal [6–8] herbertsmithite samples (see Figure 6). The theoretical result from [17,18], represented by the solid curve, traces the scaling behavior of the normalized specific heat.

It is instructive to plot the functions $T_M(B)$ and $\chi_M(B) \propto M_M^*(B)$ of $\text{ZnCu}_3(\text{OH})_6\text{Cl}_2$. These functions are displayed in Figure 8 with the data extracted from experimental facts [4]. It is seen from Figure 8a that the behavior of $T_M(B) \propto B$ is in accordance with Equation (6). It is also seen from Figure 8a that $\text{ZnCu}_3(\text{OH})_6\text{Cl}_2$ is not located exactly at the FCQPT, for $T_M(B = 0) \simeq 0.4$ K and the system demonstrate LFL behavior at $T \leq 0.4$ K [4]. Similarly, it is seen from Figure 8b that $\chi_{\text{max}}(B) \propto M_M^*(B)$, in accordance with Equations (6) and (7). Thus, the effect of the impurities on QSL can be analyzed basing on Figure 8: the LFL temperature T_{LFL} grows if QSL is shifted by impurities from the FCQPT, while the gap is absent. It also follows from Figure 8 that $\text{ZnCu}_3(\text{OH})_6\text{Cl}_2$ exhibits behavior typical of HF metals under the application of a magnetic field [16,17]. As a result, we conclude that impurities form the single integral entity with a kagome lattice at nanoscale.

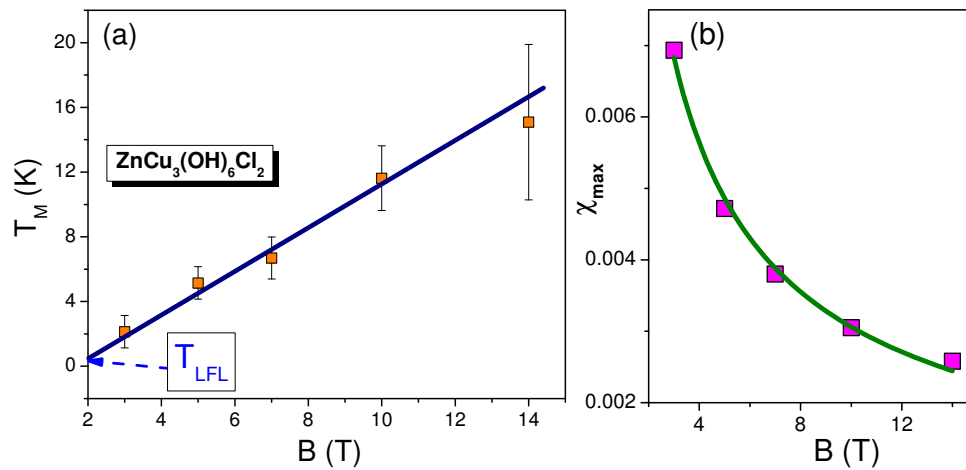


Figure 8. (Color online) Panel (a): The temperatures $T_M(B)$ at which the maxima of $\chi_{max}(B) \propto M_M^*(B)$ (see Figure 3) occur. The solid line represents the function $T_M \propto B$ (see Equation (8)). Panel (b): the maxima $\chi_{max}(B)$ of $\chi(T)$ versus B (see Figure 3). The solid curve is given by Equation (6).

The impurity model has been utilized by the authors of reference [9] to derive an intrinsic scattering measure $S_{kag}(\omega) = S_{tot}(\omega) - aS_{imp}(\omega)$. In the latter expression, $S_{tot}(\omega)$ is a total (i.e., host lattice plus impurities) scattering rate, while $S_{imp}(\omega)$ is the impurity contribution with fitting parameter a . On finding that $S_{kag}(\omega)$ goes to zero as $\omega < 0.7$ meV (see Figure 4b of reference [9]), they assert the existence of a gap. However, as we have demonstrated above, such a procedure gives just a spurious gap. Indeed, the latter conclusion relies completely on the assumption of a weak inter-impurity interaction, which is unjustified empirically since the subtraction hypothesis is negated by the experimental behavior summarized in Figure 3.

We now examine the impurity model in further detail and put its conclusion about the existence of a spin gap under scrutiny. It is seen from Figure 3 that normal low-temperature Fermi liquid properties of the magnetic susceptibility χ are confirmed experimentally at least for $B \geq 3$ T. In such strong magnetic fields and low temperatures, the impurity spins are aligned completely along the field direction. They do not have degrees of freedom, permitting them to demonstrate Curie–Weiss behavior. Thus, assuming that impurity spins are fully aligned along the magnetic field direction and hence do not contribute to χ , one remains with $\chi_{kag}(T) = \chi(T)$. Similar properties of the heat capacity follow from Figure 6. In the above magnetic fields, C_{mag}/T also demonstrates ordinary Fermi liquid behavior. This shows that at low temperatures and $B \geq 3$ T, the impurities show minute contributions to χ and C_{mag}/T . It becomes obvious that the main contribution in such a case comes from the host kagome lattice [9,24,25]. Moreover, the impurity model implies that both $\chi(T)$ and $C_{mag}(T)/T$ approach zero at $T \rightarrow 0$ and $B \geq 3$ T. It is clear from Figures 3, 4, 6, and 7 that this is not true. Namely, both χ and C_{mag}/T do not go to zero at $T \rightarrow 0$ up to $B \sim 14$ T. Moreover, the scaling properties of C_{mag}/T from Figure 7 and the behavior of both $T_M(B)$ and $\chi_{max}(B)$ displayed in Figure 8 confirm clearly the lack of a gap. The results of C_{mag} measurements [4–8] are the same for powder and bulk samples (see Figure 6).

The aforementioned experimental results are consistent with the hypothesis that the vast majority of physical properties of herbertsmithite are due to stable SCQSL. First, there is no substantial gap in the spinon excitation spectrum. Moreover, the application of high magnetic fields 18 T does not trigger such a gap. This implies that the impurity model is inadequate. These findings are in conformity with recent measurements stating that the low-temperature plateau in the local susceptibility identifies the spin-liquid ground state as a gapless one [53], while recent theoretical analysis confirms the absence of a gap [22].

4. Dynamic, Relaxation, and Heat Transport Properties

Neutron scattering measurements are one more confirmation of our hypothesis' validity. Recently, the dynamic spin susceptibility $\chi(\mathbf{q}, \omega, T) = \chi'(\mathbf{q}, \omega, T) + i\chi''(\mathbf{q}, \omega, T)$ has been measured by neutrons scattering as a function of \mathbf{q} (momentum), ω (frequency), and T . At low temperatures, the results are consistent with the idea that these quasiparticles are spinons, which form an approximately flat band [54].

The imaginary part $\chi''(T, \omega_1)$ satisfies the equation [17,19]

$$T^{2/3}\chi''(T, \omega_1) \simeq \frac{a_1\omega_1}{1 + a_2\omega_1^2}, \quad (11)$$

where a_1 and a_2 are constants and $\omega_1 = \omega/(T)^{2/3}$. Equation (11) demonstrates that $T^{2/3}\chi''(T, \omega_1)$ has a maximum $(T^{2/3}\chi''(T, \omega_1))_{\max}$ at some ω_{\max} . Equation (11) describes the scaling properties of $\chi''T^{0.66}$ established in measurements in reference [3]. As in Equation (7), we introduce the dimensionless function $(T^{2/3}\chi'')_N = T^{2/3}\chi''/(T^{2/3}\chi'')_{\max}$ and the (dimensionless) variable $E_N = \omega_1/\omega_{\max}$. In this case, Equation (11) is modified to read

$$(T^{2/3}\chi'')_N \simeq \frac{b_1E_N}{1 + b_2E_N^2}, \quad (12)$$

where b_1 and b_2 are fitting parameters. They should be chosen from the condition that the right-hand side of Equation (12) should reach the maximum at $E_N = 1$. This means that the expression $(T^{2/3}\chi'')_N = T^{2/3}\chi''/(T^{2/3}\chi'')_{\max}$ exhibits scaling as a function of E_N [17,19]. In other words, we find that $B^{2/3}\chi''(\omega)$ (cf. Equation (6)) exhibits the scaling behavior with $E_N = \omega_1/\omega_{\max}$:

$$(B^{2/3}\chi'')_N \simeq \frac{d_1E_N}{1 + d_2E_N^2}. \quad (13)$$

Similarly, d_1 and d_2 are fitting parameters chosen from the condition that the function $(B^{2/3}\chi'')_N = 1$ at $E_N = 1$. In the FCQPT point, the discussed scaling is valid almost to $T = 0$.

Figure 9 reports the function $(T^{2/3}\chi'')_N$ extracted from neutron-scattering measurements on the HF metal $\text{Ce}_{0.925}\text{La}_{0.075}\text{Ru}_2\text{Si}_2$ [55]. The corresponding data collected on two systems, $\text{ZnCu}_3(\text{OH})_6\text{Cl}_2$ [3] and $(\text{D}_3\text{O})\text{Fe}_3(\text{SO}_4)_2(\text{OD})_6$ [56], are reported in Figures 10 and 11. The figures show pretty good agreement between theoretical [19] (solid curves) and experimental results on all considered chemical compounds over almost three decades in the scaled variable E_N . Hence $(T^{2/3}\chi'')_N$ also has scaling properties. This shows that the spinons in both $\text{ZnCu}_3(\text{OH})_6\text{Cl}_2$ and $(\text{D}_3\text{O})\text{Fe}_3(\text{SO}_4)_2(\text{OD})_6$ demonstrate the same itinerant behavior as the conduction electrons in the heavy fermion compound $\text{Ce}_{0.925}\text{La}_{0.075}\text{Ru}_2\text{Si}_2$. The detection of the above itinerant behavior is very important as it convincingly shows the presence of a gapless SCQSL in herbertsmithite [17,19,20].

Under the assumption that a fermion condensate (FC) is present in the above HF metals, the imaginary part $\chi''(T, \omega)$ of the susceptibility reads [16,17]

$$T\chi''(T, \omega) \simeq \frac{a_5E}{1 + a_6E^2}, \quad (14)$$

where $E = \omega/k_B T$, while a_5 and a_6 are adjustable parameters. Expression (14) shows that $T\chi''(T, \omega)$ is a function of a single variable $E = \omega/k_B T$. In this case, the expressions (12) and (14) define two types of scaling in $\chi''(\omega, T)$. The dynamic susceptibility ($T\chi''$) taken from inelastic neutron scattering measurements on the HF metal YbRh_2Si_2 [57] is reported in Figure 12. The scaling in $(T\chi'')$ is clearly seen in both this function and variable E . This confirms both the feasibility of Equation (14) and the similarity of the HF metals and frustrated magnets properties. The scaled data acquired in measurements on such structurally different strongly correlated systems as $\text{ZnCu}_3(\text{OH})_6\text{Cl}_2$,

$\text{Ce}_{0.925}\text{La}_{0.075}\text{Ru}_2\text{Si}_2$, $(\text{D}_3\text{O})\text{Fe}_3(\text{SO}_4)_2(\text{OD})_6$, and YbRh_2Si_2 merge in a single curve over almost three decades in the scaled variables, thus confirming that these strongly correlated Fermi systems exhibit universal scaling behavior and are symptomatic of the existence of a new state of matter [17,58]. This observation strengthens the credibility of the FC approach as it can reliably explain the experimental data concerned and has demonstrable predictive power [17,35,58].

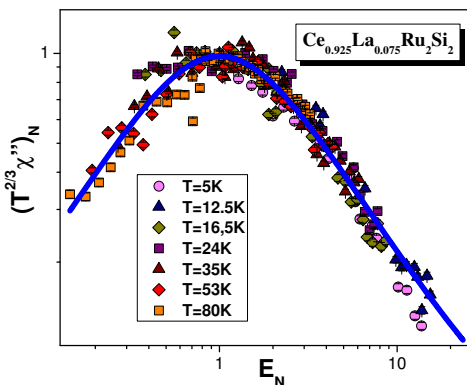


Figure 9. (Color online) Normalized dynamic spin susceptibility $(T^{2/3}\chi'')_N$, showing scaling properties. The data are taken from those on the HF metal $\text{Ce}_{0.925}\text{La}_{0.075}\text{Ru}_2\text{Si}_2$ [55]. The full line is defined by Equation (12) [19].

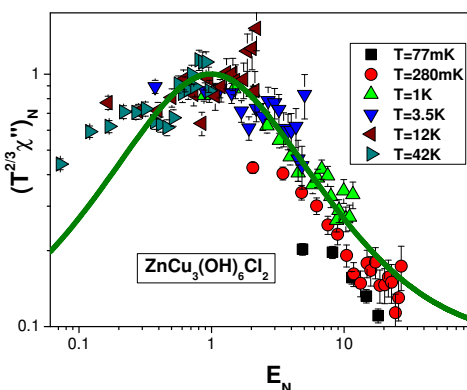


Figure 10. (Color online) Same as in Figure 9 but for herbertsmithite $\text{ZnCu}_3(\text{OH})_6\text{Cl}_2$ [3]. The full line is once more defined by Equation (12) [17,19].

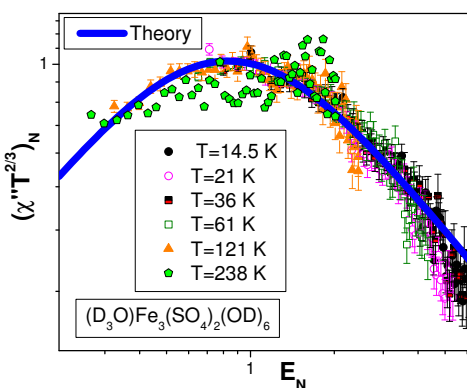


Figure 11. (Color online) Same as in Figure 9 but for deuterium jarosite $(\text{D}_3\text{O})\text{Fe}_3(\text{SO}_4)_2(\text{OD})_6$ [56]. The full line is once more defined by Equation (12) [17,19].

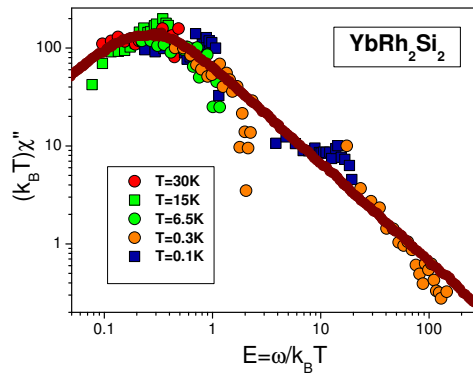


Figure 12. (Color online) Normalized dynamic spin susceptibility $T\chi''$ against $E = \omega/k_B T$. Data are taken from those on YbRh_2Si_2 [57]. The full line is defined by Equation (14) [17,19].

Indeed, it is apparent from Figures 9–12 that the calculations within the FC approach are in conformity with the experimental results, providing strong evidence that SCQSL is the underlying mechanism defining the properties of $\text{ZnCu}_3(\text{OH})_6\text{Cl}_2$ and $(\text{D}_3\text{O})\text{Fe}_3(\text{SO}_4)_2(\text{OD})_6$. We conclude that the spin gap apprehension is a rather artificial construction, which may contradict the acquired experimental knowledge about the $\text{ZnCu}_3(\text{OH})_6\text{Cl}_2$ properties. The consistency of this description based on a FCQPT as the driving mechanism for the properties of herbertsmithite at low temperature can also be taken as strong evidence against the spin gap existence in this system. Note that the presence or absence of a spin gap is not that important as it does not define the physical properties of $\text{ZnCu}_3(\text{OH})_6\text{Cl}_2$. In particular, neither χ nor C_{mag}/T vanishes in the high magnetic fields, eliminating the contribution coming from the impurities (see Figures 3, 4, 6, and 7). Moreover, Figure 10 shows that such a gap does not contribute to the imaginary part of the magnetic susceptibility, which does not vanish at the lowest temperatures. Rather, all above physical properties are due to the SCQSL. This fact can be tested by magnetic field heat transport measurements similar to organic insulators $\text{EtMe}_3\text{Sb}[\text{Pd}(\text{dmit})_2]_2$ and $\kappa - (\text{BEDT} - \text{TTF})_2\text{Cu}_2(\text{CN})_3$ [21,59,60]. Heat transport measurements are notably important as they probe the SCQSL excitations in $\text{ZnCu}_3(\text{OH})_6\text{Cl}_2$. They can also detect the itinerant spinons, which are the primary reason for heat transport. It is obvious that the above heat transport cannot do without phonons. On the other hand, the phonon contribution is barely affected by the magnetic field. To summarize, we anticipate that magnetic field dependence of heat transport measurements may be an important step forward to identify the SCQSL nature in $\text{ZnCu}_3(\text{OH})_6\text{Cl}_2$ [17,20,21].

Note that if we set the electronic charge to zero, the SCQSL in herbertsmithite becomes identically similar to the itinerant electrons ensemble in HF metals. In this case, the SCQSL thermal resistivity w reads [17,20,21]

$$w - w_0 = W_r T^2 \propto \rho - \rho_0 \propto (M^*)^2 T^2, \quad (15)$$

where $W_r T^2$ comes from spinon–spinon scattering, which is similar to the contribution AT^2 from electron–electron scattering to charge transport. Here, M^* is the effective mass and ρ is the longitudinal magnetoresistivity (LMR), while w_0 and ρ_0 denote the residual thermal and electric resistivity, respectively.

Finally, we consider the magnetic field influence on the spin-lattice relaxation rate $1/(T_1 T)$. Figure 13A shows the normalized quantity $1/(T_1 T)_N$ as a function of the magnetic field. It shows that with a magnetic field increase, $1/(T_1 T)$ decays progressively. Contrary to the previous cases, where the normalization has been fulfilled in the point of maximum, here we normalize our curves in the inflection point, $B = B_{\text{inf}}$, marked by the arrows in the main panel and inset. The same procedure has been performed with the normalized magnetoresistance shown in the inset to Figure 13. The relation $1/(T_1 T)_N \propto (M^*)^2$ shows that our system located near its QCP would exhibit similar behavior of $1/(T_1 T)_N$ [16,17,20,21]. Significantly, Figure 13A shows that the normalized spin-lattice relaxation rate of herbertsmithite [61] and the HF metal $\text{YbCu}_{5-x}\text{Au}_x$ [62] do exhibit the same behavior. As seen from

Figure 13A for $B \leq B_{\text{inf}}$ (or $B_N \leq 1$), the quantity $1/(T_1T)_N$ is almost magnetic-field-independent. At the same time, at elevated magnetic fields it decays [16,17,20,21] according to

$$W_r \propto 1/(T_1T)_N = \rho_N \propto (M^*)^2 \propto B^{-4/3}. \quad (16)$$

Thus, we hypothesize that magnetic field B yields a crossover between NFL and LFL regimes. It also reduces substantially the relaxation rate as well as the thermal resistivity, similar to the case of the normalized LMR of YbRh_2Si_2 , (see Figure 13B). Experimental data for the LMR is taken from [63]. Also of high priority are measurements of low-energy inelastic neutron scattering on $\text{ZnCu}_3(\text{OH})_6\text{Cl}_2$ crystalline samples under the application of a magnetic field, driving the system into the LFL sector of the phase diagram (see Figure 2). The latter measurements permit direct observation of a possible gap, since in this case the impurity contribution is insignificant.

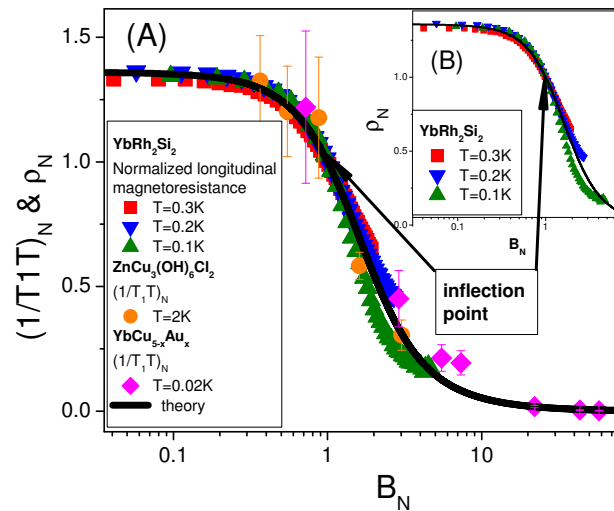


Figure 13. (Color online) Main panel (A). Magnetic field dependence of normalized spin-lattice relaxation rate $(1/T_1T)_N$. Data for different substances are shown by different markers: solid squares correspond to $\text{ZnCu}_3(\text{OH})_6\text{Cl}_2$ [61] and solid triangles to $\text{YbCu}_{5-x}\text{Au}_x$ at $x = 0.4$ [62]. The normalization is done in the inflection point, shown by the arrow. Inset (B). Same as in main panel (A), but for the normalized magnetoresistance ρ_N , for YbRh_2Si_2 at different temperatures [63] (legend) coded by symbols. The results of calculations are shown in both panels by the full line, defining the scaling behavior of $W_r \propto (M^*)^2$ (see Equations (15) and (16)).

Recent neutron-scattering measurements on YbMgGaO_4 reveal broad spin excitations covering a wide region of the Brillouin zone, thereby favoring the existence of a spinon Fermi surface [64,65]. At the same time, the measurements of heat transport do not show any substantial magnetic excitation contributions to thermal conductivity, thus raising doubt as to the presence of a QSL [66]. We speculate that the observed behavior can be attributed to the emergence of a Mott insulator (see e.g., [67]), placing the system beyond the FCQPT point in the phase diagram. At the same time, in the case of herbertsmithite, the transport and thermodynamic properties suggest that the gapless state represented by the SCQSL is situated before the FCQFT. We note that recent theoretical studies of possible gaps in the ground state of herbertsmithite lead to quite different conclusions about the presence of a gap [18,22,68–70]. Recent experimental studies also indicate that the spin-liquid ground state in kagome lattice is gapless [53], and that two distinct types of defects in herbertsmithite are found [71]. This observation makes the impurity model vulnerable. Therefore, to probe QSL in herbertsmithite reliably, it is of crucial importance to carry out the experimental studies suggested above.

5. Charge Transport and Optical Conductivity

Our next step is the analysis of the herbertsmithite optical conductivity $\bar{\sigma}$ at low frequencies. To avoid the contribution of phonon absorption to the conductivity, we consider low temperatures T and frequencies ω [33]. Under such assumptions, we can neglect the lattice symmetry (kagome vs. triangular) as the wavelength is much larger than the typical crystal size. In atomic units $\hbar = c = 1$, the Hamiltonian of a particle having momentum $\mathbf{p} = i\nabla$, spin \mathbf{s} , and charge e is given by

$$\hat{H} = \frac{1}{2m} (\mathbf{p} - e\mathbf{A})^2 + e\phi - \frac{\mu_B}{s} \mathbf{s} \cdot \mathbf{B}, \quad (17)$$

where \mathbf{A} and ϕ are the vector and scalar potentials, respectively. The nature of the vector potential $\nabla \cdot \mathbf{A} = 0$ implies that \mathbf{p} and \mathbf{A} operators commute. Since for spinons, $e = 0$, only the last term on the right-hand side of Equation (17) contributes to $\bar{\sigma}$.

Equations (5) and (11) show that at small ω , the imaginary part of the spin susceptibility reads [19]

$$\chi''(\omega) \propto \omega(M^*)^2. \quad (18)$$

Observing that the energy transfer ε_B [36,43] between magnetic field $B(\omega)$ and our system is due to the last term in Equation (17), we obtain

$$\varepsilon_B = 2\pi\omega \left[\frac{\mu_B}{s} \mathbf{s} \cdot \mathbf{B} \right] \chi''(\omega) \equiv 2\pi \frac{\omega^2 \mu_B^3}{s} (M^*)^2 \mathbf{s} \cdot \mathbf{B}. \quad (19)$$

The same quantity, ε_E , coming from the electric field $E(\omega)$, reads

$$\varepsilon_E = E^2(\omega) \bar{\sigma}(\omega). \quad (20)$$

Comparison of Equations (19) and (20) yields

$$\bar{\sigma}(\omega) \propto \omega \chi''(\omega) \propto \omega^2 (M^*)^2. \quad (21)$$

It follows from Equation (21) that $\bar{\sigma}(\omega) \propto \omega^2$, and that behavior is consistent with experimental facts obtained in measurements on $\text{ZnCu}_3(\text{OH})_6\text{Cl}_2$ and $\text{EtMe}_3\text{Sb}[\text{Pd}(\text{dmit})_2]_2$, representing the best candidates for identification as materials that host QSL [2,33,72]. We note that χ'' (18) at low ω coincides Equation (11) and provides a good description of the experimental data (see Figures 9 and 10). Equations (5) and (21) inform us that at elevated temperatures, $\bar{\sigma}(T)$ is a decreasing function, which conforms with the experimental data [33]. It also follows from Equations (6) and (21) that $\bar{\sigma}(\omega, B)$ is a decreasing function of B . This observation seems to be contradictory as no systematic B dependence is observed experimentally [33].

To elucidate the $\bar{\sigma}(B)$ behavior, we note that corresponding experiments have been performed at $T = 3$ K and $B \leq 7$ T [33]. This means that the system is still in the transition region of the phase diagram and does not yet have the normal Fermi liquid properties, where the effective mass M^* is given by Equation (6). In this case, the effective mass properties is due to Equation (5), rather than Equation (6). This means that the dependence $\bar{\sigma}(B)$ cannot be observed. Accordingly, we think that substantial $\bar{\sigma}(B)$ dependence can be observed at $B \simeq 7$ T in the case of $T \leq 1$ K. In that case, as one sees from Figure 6, the effective mass $M^* \propto C_{\text{mag}}/T$ is a diminishing function of the applied magnetic field. Thus, we predict that $\bar{\sigma}(B)$ diminishes with growing magnetic fields, as follows from Equations (6) and (21). Since the contribution coming from phonons does not depend on the magnetic field, we propose that measurements of the variation $\delta\sigma$, i.e., $\delta\sigma = \bar{\sigma}(\omega, B) - \bar{\sigma}(\omega, B = 0)$, can reveal both the physics of SCQSL and the ground state of $\text{ZnCu}_3(\text{OH})_6\text{Cl}_2$, as well as the ground state of other materials hosting a QSL. The above experiments on measurements of the heat transport and optical conductivity can be carried out on samples with varying x . Such experiments yield information

on the influence of impurities on the value of the gap. We predict that at moderate $x \sim 20\%$, the SCQSL remains robust, for both inhomogeneity and randomness facilitate frustration.

6. Summary

The central message of this review is that to achieve a satisfactory understanding of the quantum spin-liquid physics of herbertsmithite at the nanoscale, it is essential to perform the targeted measurements on $\text{ZnCu}_3(\text{OH})_6\text{Cl}_2$ that we have discussed. These focus on heat transport, low-energy inelastic neutron scattering, and optical conductivity $\bar{\sigma}$, in the presence of magnetic fields at low temperatures. Moreover, we have suggested that the increasing x , i.e., the percentage of Zn sites that are occupied by Cu, can facilitate the frustration of the lattice and thereby act to stabilize the quantum spin liquid state. This conjecture can be tested in experiments on samples of herbertsmithite with different x values under the application of a magnetic field. To be specific, the results of the measurements might yield an unambiguous answer to the question of whether the gap in spinon excitations really exists, and if so, how it depends on impurities. In addition, such experiments will help to separate the universal effects from those coming both from phonons and from the impurities that pollute each specific sample of the material, and to represent frustrated magnets with SCQSL as the new state of matter that exhibits the properties of HF metals, with one exception: these are insulators and do not support the charge current.

Other results reported in our review paper are based on the description of low-frequency optical conductivity experimental data on herbertsmithite. For that, we implied that $\text{ZnCu}_3(\text{OH})_6\text{Cl}_2$ is a system of strongly correlated fermions with properties defined primarily by a quantum spin liquid of chargeless spinons. We have also predicted the optical conductivity dependence on the magnetic field and pointed out the explicit conditions under which such a dependence can be experimentally observed. While making a step towards the confirmation of the existence of the SCQSL state in $\text{ZnCu}_3(\text{OH})_6\text{Cl}_2$, our considerations may also pave the way to studies of this state in other magnetic frustrated insulators at the nanoscale.

Author Contributions: V.R.S., V.A.S., A.Z.M., and M.Y.A. designed the project and directed it with the help of J.W.C., G.S.J. and Y.S.L. Y.S.L. performed the calculations. V.R.S., V.A.S. and J.W.C. wrote the manuscript and all authors commented on it. The manuscript reflects the contributions of all authors.

Funding: This research received no external funding.

Acknowledgments: This work was partly supported by U.S. DOE, Division of Chemical Sciences, Office of Basic Energy Sciences, Office of Energy Research. JWC acknowledges support from the McDonnell Center for the Space Sciences and expresses gratitude to the University of Madeira and its branch of Centro de Investigação em Matemática e Aplicações (CIMA) for their gracious hospitality during periods of extended residence.

Conflicts of Interest: The authors declare no conflict of interest.

References

1. Pustogow, A.; Li, Y.; Voloshenko, I.; Pupal, P.; Krellner, C.; Mazin, I.I.; Dressel, M.; Valentí, R. Nature of optical excitations in the frustrated kagome compound herbertsmithite. *Phys. Rev.* **2017**, *96*, 241114(R). [[CrossRef](#)]
2. Sushkov, A.B.; Jenkins, G.S.; Han, T.-H.; Lee, Y.S.; Drew, H.D. Infrared phonons as a probe of spin-liquid states in herbertsmithite $\text{ZnCu}_3(\text{OH})_6\text{Cl}_2$. *Phys. Condens. Matter* **2017**, *29*, 095802. [[CrossRef](#)] [[PubMed](#)]
3. Helton, J.S.; Matan, K.; Shores, M.P.; Nytko, E.A.; Bartlett, B.M.; Qiu, Y.; Nocera, D.G.; Lee, Y.S. Dynamic Scaling in the Susceptibility of the Spin-1/2 Kagome Lattice Antiferromagnet Herbertsmithite. *Phys. Rev. Lett.* **2010**, *104*, 147201. [[CrossRef](#)] [[PubMed](#)]
4. Helton, J.S.; Matan, K.; Shores, M.P.; Nytko, E.A.; Bartlett, B.M.; Yoshida, Y.; Takano, Y.; Suslov, A.; Qiu, Y.; Chung, J.-H.; et al. Spin Dynamics of the Spin-1/2 Kagome Lattice Antiferromagnet $\text{ZnCu}_3(\text{OH})_6\text{Cl}_2$. *Phys. Rev. Lett.* **2007**, *98*, 107204. [[CrossRef](#)] [[PubMed](#)]
5. De Vries, M.A.; Kamenev, K.V.; Kockelmann, W.A.; Sanchez-Benitez, J.; Harrison, A. Magnetic Ground State of an Experimental $S = 1/2$ Kagome Antiferromagnet. *Phys. Rev. Lett.* **2008**, *100*, 157205. [[CrossRef](#)] [[PubMed](#)]

6. Han, T.H.; Helton, J.S.; Chu, S.; Prodi, A.; Singh, D.K.; Mazzoli, C.; Müller, P.; Nocera, D.G.; Lee, Y.S. Synthesis and characterization of single crystals of the spin-1/2 kagome-lattice antiferromagnets $Zn_xCu_{4-x}(OH)_6Cl_2$. *Phys. Rev. B* **2011**, *83*, 100402(R). [[CrossRef](#)]
7. Han, T.H.; Chu, S.; Lee, Y.S. Refining the Spin Hamiltonian in the Spin-1/2 Kagome Lattice Antiferromagnet $ZnCu_3(OH)_6Cl_2$ Using Single Crystals. *Phys. Rev. Lett.* **2012**, *108*, 157202. [[CrossRef](#)] [[PubMed](#)]
8. Han, T.H.; Chisnell, R.; Bonnoit, C.J.; Freedman, D.E.; Zapf, V.S.; Harrison, N.; Nocera, D.G.; Takano, Y.; Lee, Y.S. Thermodynamic Properties of the Quantum Spin Liquid Candidate $ZnCu_3(OH)_6Cl_2$ in High Magnetic Fields. *arXiv* **2014**, arXiv:1402.2693.
9. Han, T.H.; Norman, M.R.; Wen, J.-J.; Rodriguez-Rivera, J.A.; Helton, J.S.; Broholm, C.; Lee, Y.S. Correlated impurities and intrinsic spin-liquid physics in the kagome material herbertsmithite. *Phys. Rev. B* **2016**, *94*, 060409(R). [[CrossRef](#)]
10. Paddison, J.A.M.; Daum, M.; Dun, Z.; Ehlers, G.; Liu, Y.; Stone, M.B.; Zhou, H.; Mourigal, M. Continuous excitations of the triangular-lattice quantum spin liquid $YbMgGaO_4$. *Nat. Phys.* **2017**, *13*, 117. [[CrossRef](#)]
11. Saito, Y.; Minamidate, T.; Kawamoto, A.; Matsunaga, N.; Nomura, K. Site-specific ^{13}C NMR study on the locally distorted triangular lattice of the organic conductor $\kappa - (BEDT - TTF)_2Cu_2(CN)_3$. *Phys. Rev. B* **2018**, *98*, 205141. [[CrossRef](#)]
12. Lazic, P.; Pinteric, M.; Góngora, D.R.; Pustogow, A.; Treptow, K.; Ivek, T.; Milat, O.; Gumhalter, B.; Clić, N.; Dressel, M.; et al. Importance of van der Waals interactions and cation-anion coupling in an organic quantum spin liquid. *Phys. Rev. B* **2018**, *97*, 245134. [[CrossRef](#)]
13. Pinterić, M.; Gongora, D.R.; Rapljenović, Z.; Ivek, T.; Culo, M.; Korin-Hamzić, B.; Milat, O.; Gumhalter, B.; Lazić, P.; Alonso, M.S.; et al. Electrodynamics in Organic Dimer Insulators Close to Mott Critical Point. *Crystals* **2018**, *8*, 190. [[CrossRef](#)]
14. Shi, Z.; Steinhardt, W.; Graf, D.; Corboz, P.; Weickert, F.; Harrison, N.; Jaime, M.; Marjerrison, C.; Dabkowska, H.A.; Mila, F.; et al. Emergent bound states and impurity pairs in chemically doped Shastry-Sutherland system. *Nat. Commun.* **2019**, *10*, 2439. [[CrossRef](#)]
15. Yamaguchi, H.; Okada, M.; Kono, Y.; Kittaka, S.; Sakakibara, T.; Okabe, T.; Iwasaki, Y.; Hosokoshi, Y. Randomness-induced quantum spin liquid on honeycomb lattice. *Sci. Rep.* **2017**, *7*, 16144. doi:10.1038/s41598-017-16431-0. [[CrossRef](#)]
16. Shaginyan, V.R.; Amusia, M.Y.; Msezane, A.Z.; Popov, K.G. Scaling behavior of heavy fermion metals. *Phys. Rep.* **2010**, *492*, 31–109. [[CrossRef](#)]
17. Amusia, M.Y.; Popov, K.G.; Shaginyan, V.R.; Stephanovich, V.A. *Theory of Heavy-Fermion Compounds*; Springer Series in Solid-State Sciences; Springer: Berlin/Heidelberg, Germany, 2014; Volume 182.
18. Shaginyan, V.R.; Msezane, A.Z.; Popov, K.G. Thermodynamic properties of the kagome lattice in herbertsmithite. *Phys. Rev. B* **2011**, *84*, 060401(R). [[CrossRef](#)]
19. Shaginyan, V.R.; Msezane, A.Z.; Popov, K.G.; Khodel, V.A. Scaling in dynamic susceptibility of herbertsmithite and heavy-fermion metals. *Phys. Lett. A* **2012**, *376*, 2622–2626. [[CrossRef](#)]
20. Shaginyan, V.R.; Msezane, A.Z.; Popov, K.G.; Japaridze, G.S.; Stephanovich, V.A. Identification of strongly correlated spin liquid in herbertsmithite. *Europhys. Lett.* **2012**, *97*, 56001. [[CrossRef](#)]
21. Shaginyan, V.R.; Msezane, A.Z.; Popov, K.G.; Japaridze, G.S.; Khodel, V.A. Heat transport in magnetic fields by quantum spin liquid in the organic insulators $EtMe_3Sb[Pd(dmit)_2]_2$ and $\kappa - (BEDT - TTF)_2Cu_2(CN)_3$. *Europhys. Lett.* **2013**, *103*, 67006. [[CrossRef](#)]
22. Liao, H.J.; Xie, Z.Y.; Chen, J.; Liu, Z.Y.; Xie, H.D.; Huang, R.Z.; Normand, B.; Xiang, T. Gapless Spin-Liquid Ground State in the $S = 1/2$ Kagome Antiferromagnet. *Phys. Rev. Lett.* **2017**, *118*, 137202. [[CrossRef](#)]
23. Shaginyan, V.R.; Amusia, M.Y.; Msezane, A.Z.; Popov, K.G.; Stephanovich, V.A. Heavy fermion spin liquid in herbertsmithite. *Phys. Lett. A* **2015**, *379*, 2092–2096. [[CrossRef](#)]
24. Fu, M.; Imai, T.; Han, T.H.; Lee, Y.S. Evidence for a gapped spin-liquid ground state in a kagome Heisenberg antiferromagnet. *Science* **2015**, *350*, 655–658. [[CrossRef](#)]
25. Imai, T.; Fu, M.; Han, T.H.; Lee, Y.S. Local spin susceptibility of the $S = 1/2$ kagome lattice in $ZnCu_3(OH)_6Cl_2$. *Phys. Rev. B* **2011**, *84*, 020411(R). [[CrossRef](#)]
26. Norman, M.R. Herbertsmithite and the search for the quantum spin liquid. *Rev. Mod. Phys.* **2016**, *88*, 041002. [[CrossRef](#)]
27. Zhou, Y.; Kanoda, K.; Ng, T.-K. Quantum spin liquid states. *Rev. Mod. Phys.* **2017**, *89*, 025003. [[CrossRef](#)]
28. Savary, L.; Balents, L. Quantum spin liquids: A review. *Rep. Prog. Phys.* **2017**, *80*, 016502. [[CrossRef](#)]

29. Feng, Z.; Li, Z.; Yi, X.M.W.; Wi, Y.; Zhang, J.; Wang, Y.-C.; Jiang, W.; Liu, Z.; Li, S.; Liu, F.; et al. Gapped Spin-1/2 Spinon Excitations in a New Kagome Quantum Spin Liquid Compound $\text{Cu}_3\text{Zn}(\text{OH})_6\text{FBr}$. *Chin. Phys. Lett.* **2017**, *34*, 077502. [[CrossRef](#)]
30. Khodel, V.A.; Shaginyan, V.R. Superfluidity in system with fermion condensate. *JETP Lett.* **1990**, *51*, 553–555.
31. Khodel, V.A.; Shaginyan, V.R.; Khodel, V.V. New approach in the microscopic Fermi system theory. *Phys. Rep.* **1994**, *249*, 1–134. [[CrossRef](#)]
32. Volovik, G.E. Quantum Phase Transitions from Topology in Momentum Space. In *Quantum Analogues: From Phase Transitions to Black Holes and Cosmology*; Springer: Berlin/Heidelberg, Germany, 2007; Volume 718, pp. 31–73.
33. Pilon, D.V.; Lui, C.H.; Han, T.-H.; Shrekenhamer, D.; Frenzel, A.J.; Padilla, W.J.; Lee, Y.S.; Gedik, N. Spin-Induced Optical Conductivity in the Spin-Liquid Candidate Herbertsmithite. *Phys. Rev. Lett.* **2013**, *111*, 127401. [[CrossRef](#)]
34. Potter, A.C.; Senthil, T.; Lee, P.A. Mechanisms for sub-gap optical conductivity in Herbertsmithite. *Phys. Rev. B* **2013**, *87*, 245106. [[CrossRef](#)]
35. Shaginyan, V.R.; Stephanovich, V.A.; Msezane, A.Z.; Schuck, P.; Clark, J.W.; Amusia, M.Y.; Japaridze, G.S.; Popov, K.G.; Kirichenko, E.V. New State of Matter: Heavy Fermion Systems, Quantum Spin Liquids, Quasicrystals, Cold Gases, and High-Temperature Superconductors. *J. Low Temp. Phys.* **2017**, *189*, 410–450. [[CrossRef](#)]
36. Shaginyan, V.R.; Msezane, A.Z.; Stephanovich, V.A.; Popov, K.G.; Japaridze, G.S. Universal Behavior of Quantum Spin Liquid and Optical Conductivity in the Insulator Herbertsmithite. *J. Low Temp. Phys.* **2018**, *191*, 4–13. [[CrossRef](#)]
37. Green, D.; Santos, L.; Chamon, C. Isolated flat bands and spin-1 conical bands in two-dimensional lattices. *Phys. Rev. B* **2010**, *82*, 075104. [[CrossRef](#)]
38. Heikkilä, T.T.; Kopnin, N.B.; Volovik, G.E. Flat bands in topological media. *JETP Lett.* **2011**, *94*, 233. [[CrossRef](#)]
39. Volovik, G.E. A new class of normal Fermi liquids. *JETP Lett.* **1991**, *53*, 222.
40. Kelly, Z.A.; Gallagher, M.J.; McQueen, T.M. Electron Doping a Kagome Spin Liquid. *Phys. Rev. X* **2016**, *6*, 041007. [[CrossRef](#)]
41. Landau, L.D. The theory of a Fermi liquid. *Sov. Phys. JETP* **1956**, *3*, 920.
42. Lifshitz, E.M.; Pitaevskii, L.P. *Statisticheskaya Fizika (Statistical Physics)*; Nauka: Moscow, Russia, 1978; Pt. 2; Translated into English, Pergamon Press: Oxford, UK, 1980.
43. Pines, D.; Nozières, P. *Theory of Quantum Liquids*; Benjamin: New York, NY, USA, 1966.
44. Coleman, P. *Lectures on the Physics of Highly Correlated Electron Systems VI*; Mancini, F., Ed.; American Institute of Physics: New York, NY, USA, 2002.
45. Clark, J.W.; Zverev, M.V.; Khodel, V.A. Entropy excess in strongly correlated Fermi systems near a quantum critical point. *Ann. Phys.* **2012**, *327*, 3063–3083. [[CrossRef](#)]
46. Gegenwart, P.; Tokiwa, Y.; Westerkamp, T.; Weickert, F.; Custers, J.; Ferstl, J.; Krellner, C.; Geibel, C.; Kersch, P.; Müller, K.-H. High-field phase diagram of the heavy-fermion metal YbRh_2Si_2 . *New J. Phys.* **2006**, *8*, 171. [[CrossRef](#)]
47. Oeschler, N.; Hartmann, S.; Pikul, A.; Krellner, C.; Geibel, C.; Steglich, F. Low-temperature specific heat YbRh_2Si_2 . *Phys. B* **2008**, *403*, 1254. [[CrossRef](#)]
48. Shaginyan, V.R.; Popov, K.G.; Stephanovich, V.A.; Fomichev, V.I.; Kirichenko, E.V. High-magnetic-fields thermodynamics of the heavy-fermion metal YbRh_2Si_2 . *Europhys. Lett.* **2011**, *93*, 17008. [[CrossRef](#)]
49. Shaginyan, V.R.; Stephanovich, V.A.; Popov, K.G.; Kirichenko, E.V. Quasi-one-dimensional quantum spin liquid in the $\text{Cu}(\text{C}_4\text{H}_4\text{N}_2)(\text{NO}_3)_2$ insulator. *JETP Lett.* **2016**, *103*, 32. [[CrossRef](#)]
50. Shaginyan, V.R.; Stephanovich, V.A.; Popov, K.G.; Kirichenko, E.V.; Artamonov, S.A. Magnetic quantum criticality in quasi-one-dimensional Heisenberg antiferromagnet $\text{Cu}(\text{C}_4\text{H}_4\text{N}_2)(\text{NO}_3)_2$. *Ann. Phys.* **2016**, *528*, 483–492. [[CrossRef](#)]
51. Shaginyan, V.R.; Stephanovich, V.A.; Msezane, A.Z.; Japaridze, G.S.; Popov, K.G. The influence of topological phase transition on the superfluid density of overdoped copper oxides. *Phys. Chem. Chem. Phys.* **2017**, *19*, 21964. [[CrossRef](#)]
52. Shaginyan, V.R.; Amusia, M.Y.; Clark, J.W.; Japaridze, G.S.; Msezane, A.Z.; Popov, K.G.; Stephanovich, V.A.; Zverev, M.V.; Khodel, V.A. Comment on “Topological excitations and the dynamic structure factor of spin liquids on the kagome lattice”, *Nature Physics* 2014, *10*, 289–293. *arXiv* **2014**, arXiv:1409.4034 [[CrossRef](#)]

53. Gomilsek, M.; Klanjsek, M.; Pregelj, M.; Luetkens, H.; Li, Y.; Zhang, Q.M.; Zorko, A. μ SR insight into the impurity problem in quantum kagome antiferromagnets. *Phys. Rev. B* **2016**, *94*, 024438. [[CrossRef](#)]
54. Han, T.H.; Helton, J.S.; Chu, S.; Nocera, D.G.; Rodriguez-Rivera, J.A.; Broholm, C.; Lee, Y.S. Fractionalized excitations in the spin-liquid state of a kagome-lattice antiferromagnet. *Nature* **2012**, *492*, 406–410. [[CrossRef](#)]
55. Knafo, W.; Raymond, S.; Flouquet, J.; Fåk, B.; Adams, M.A.; Haen, P.; Lapierre, F.; Yates, S.; Lejay, P. Anomalous scaling behavior of the dynamical spin susceptibility of $\text{Ce}_{0.925}\text{La}_{0.075}\text{Ru}_2\text{Si}_2$. *Phys. Rev. B* **2004**, *70*, 174401. [[CrossRef](#)]
56. Fåk, B.; Coomer, F.C.; Harrison, A.; Visser, D.; Zhitomirsky, M.E. Spin-liquid behavior in a kagome antiferromagnet: Deuterium jarosite. *Europhys. Lett.* **2008**, *81*, 17006. [[CrossRef](#)]
57. Stock, C.; Broholm, C.; Demmel, F.; Duijn, J.V.; Taylor, J.W.; Kang, H.J.; Hu, R.; Petrovic, C. From Incommensurate Correlations to Mesoscopic Spin Resonance in YbRh_2Si_2 . *Phys. Rev. Lett.* **2012**, *109*, 127201. [[CrossRef](#)] [[PubMed](#)]
58. Shaginyan, V.R.; Msezane, A.Z.; Japaridze, G.S.; Popov, K.G.; Khodel, V.A. Strongly correlated Fermi systems as a new state of matter. *Front. Phys.* **2016**, *11*, 117103. [[CrossRef](#)]
59. Yamashita, M.; Nakata, N.; Senshu, Y.; Nagata, M.; Yamamoto, H.M.; Kato, R.; Shibauchi, T.; Matsuda, Y. Highly Mobile Gapless Excitations in a Two-Dimensional Candidate Quantum Spin Liquid. *Science* **2010**, *328*, 1246–1248. [[CrossRef](#)] [[PubMed](#)]
60. Yamashita, M.; Shibauchi, T.; Matsuda, Y. Probing non-equilibrium vibrational relaxation pathways in Quantum Spin Liquids. *Chem. Phys.* **2012**, *13*, 74.
61. Imai, T.; Nytko, E.A.; Bartlett, B.M.; Shores, M.P.; Nocera, D.G. ^{63}Cu , ^{35}Cl , and ^1H NMR in the $S = 1/2$ Kagome Lattice $\text{ZnCu}_3(\text{OH})_6\text{Cl}_2$. *Phys. Rev. Lett.* **2008**, *100*, 077203. [[CrossRef](#)] [[PubMed](#)]
62. Carretta, P.; Pasero, R.; Giovannini, M.; Baines, C. Magnetic-field-induced crossover from non-Fermi to Fermi liquid at the quantum critical point of $\text{YbCu}_{5-x}\text{Au}_x$. *Phys. Rev. B* **2009**, *79*, 020401(R). [[CrossRef](#)]
63. Gegenwart, P.; Westerkamp, T.; Krellner, C.; Tokiwa, Y.; Paschen, S.; Geibel, C.; Steglich, F.; Abrahams, E.; Si, Q. Multiple energy scales at a quantum critical point. *Science* **2007**, *315*, 969–971. [[CrossRef](#)] [[PubMed](#)]
64. Shen, Y.; Li, Y.-D.; Wo, H.; Li, Y.; Shen, S.; Pan, B.; Wang, Q.; Walker, H.C.; Steffens, P.; Boehm, M.; et al. Evidence for a spinon Fermi surface in a triangular-lattice quantum-spin-liquid candidate. *Nature* **2016**, *540*, 559–562. [[CrossRef](#)]
65. Luo, Z.-X.; Lake, E.; Mei, J.-W.; Sarykh, O.A. Spinon Magnetic Resonance of Quantum Spin Liquids. *Phys. Rev. Lett.* **2018**, *120*, 037204. [[CrossRef](#)]
66. Xu, Y.; Zhang, J.; Li, Y.S.; Yu, Y.J.; Hong, X.C.; Zhang, Q.M.; Li, S.Y. Absence of Magnetic Thermal Conductivity in the Quantum Spin-Liquid Candidate YbMgGaO_4 . *Phys. Rev. Lett.* **2016**, *117*, 267202. [[CrossRef](#)]
67. Nakayama, M.; Kondo, T.; Tian, Z.; Ishikawa, J.J.; Halim, M.; Bareille, C.; Malaeb, W.; Kuroda, K.; Tomita, T.; Ideta, S.; et al. Slater to Mott Crossover in the Metal to Insulator Transition of $\text{Nd}_2\text{Ir}_2\text{O}_7$. *Phys. Rev. Lett.* **2016**, *117*, 056403. [[CrossRef](#)]
68. Yan, S.; Huse, D.A.; White, S.R. Spin-Liquid Ground State of the $S = 1/2$ Kagome Heisenberg Antiferromagnet. *Science* **2011**, *332*, 1173–1176. [[CrossRef](#)]
69. Depenbrock, S.; McCulloch, I.P.; Schollwock, U. Nature of the Spin-Liquid Ground State of the $S = 1/2$ Heisenberg Model on the Kagome Lattice. *Phys. Rev. Lett.* **2012**, *109*, 067201. [[CrossRef](#)]
70. Jiang, H.-C.; Wang, Z.; Balents, L. Identifying topological order by entanglement entropy. *Nat. Phys.* **2012**, *8*, 902. [[CrossRef](#)]
71. Zorko, A.; Herak, M.; Gomilšek, M.; van Tol, J.; Velázquez, M.; Khuntia, P.; Bert, F.; Mendels, P. Symmetry Reduction in the Quantum Kagome Antiferromagnet Herbertsmithite. *Phys. Rev. Lett.* **2017**, *118*, 017202. [[CrossRef](#)] [[PubMed](#)]
72. Pustogow, A.; Saito, Y.; Zhukova, E.; Gorshunov, B.; Kato, R.; Lee, T.-H.; Dobrosavljević, V.; Dressel, M. Low-Energy Excitations in Quantum Spin Liquids Identified by Optical Spectroscopy. *Phys. Rev. Lett.* **2018**, *121*, 056402. [[CrossRef](#)] [[PubMed](#)]

